Materials Transactions, Vol. 48, No. 11 (2007) pp. 2973 to 2977

EXPRESS REGULAR ARTICLE

Effect of Chromium Content on Corrosion Behaviors of Fe-9Al-30Mn-(3,5,6.5,8)Cr-1C Alloys

Cheng Shun Wang*[1], Cheng Yao Tsai*[1], Chuen Guang Chao and Tzeng Feng Liu*[2]

Department of Materials Science and Engineering, National Chiao Tung University, 1001 Ta Hsueh Road, Hsinchu 30049, Taiwan, R. O. China

The corrosion behaviors of the as-quenched austenitic Fe-9%Al-30%Mn-(3,5,6.5,8)%Cr-1%C (in mass%) alloys in 3.5% NaCl solution have been examined. Passivation could be observed for all of the four alloys. The corrosion potential (E_{corr}) and pitting potential (E_{pp}) increased pronouncedly as Cr content increased from 3 to 5%, and decreased as Cr content up to 6.5 and 8%. The decrease of E_{corr} and E_{pp} of alloys containing 6.5 and 8% Cr was due to the formation of $(Fe,Mn,Cr)_7C_3$ carbides within the austenite matrix and on the grain boundaries. The present result indicates that the Fe-9%Al-30%Mn-5%Cr-1%C alloy exhibited the highest corrosion resistance in 3.5% NaCl solution. It is worthy to note that the corrosion behaviors of the austenitic FeAlMnCrC alloys with higher Cr ($\geq$ 3%) content have never been reported in previous literature. [doi:10.2320/matertrans.MER2007138]

(Received June 20, 2007; Accepted July 18, 2007; Published October 11, 2007)

Keywords: *austenitic iron aluminum manganese chromium carbon alloys, corrosion resistance alloys, sodium chloride solution, electrochemical polarization*

1. Introduction

In previous studies,[1–6] it is clear that fully austenitic Fe-(7.8–10.0)%Al-(28.0–32.2)%Mn-(0.86–1.30)%C alloys could posses excellent mechanical properties. However, the corrosion resistance of the austenitic FeAlMnC alloys in aqueous environments was not adequate for the applications in industry.[5–13] Since carbon was reported to be detrimental to the corrosion resistance,[9] reducing the carbon content may be an effective way to improve the corrosion resistance of the FeAlMnC alloys. However, it was found that with lower C content, the Fe-(8.9–10.5)%Al-(24.0–30.0)%Mn-(0.21–0.50)%C alloys consisted of (austenite (γ) + ferrite (α)) dual phases.[6,13–17] The corrosion resistance of the dual-phase FeAlMnC alloys was worse than that of the austenitic FeAlMnC alloys.[6,13,14] The reason was that in the dual-phase FeAlMnC alloys, pitting was the primary type of corrosion and it took place preferentially within the α grains and on the γ/α grain boundaries.[6,13,14]

In order to improve the corrosion resistance, 3.1$\sim$6.2% Cr has been added to the dual-phase Fe-(8.9–9.9)%Al-(21.5–27.7)%Mn-(0.33–0.42)%C alloys.[13,15] Consequently, it was found that the addition of Cr was not very effective in the improvement of the corrosion resistance of the dual-phase FeAlMnC alloys. Furthermore, it was also reported that the mechanical properties of the dual-phase FeAlMnCrC alloys were far inferior to those of austenitic ones. Therefore, it is expected that a proper combination of chromium and carbon contents to form fully austenitic FeAlMnCrC alloys is a probable method to improve the corrosion resistance without significant loss in strength. The corrosion resistance of austenitic Fe-(8.4–8.9)%Al-(29.5–31.3)%Mn-(2.6–2.8)%Cr-(0.98–1.06)%C alloys have also been examined by several researchers.[5,6] In their studies, it was obviously seen that the corrosion resistance of the austenitic FeAlMnCrC alloys was indeed superior to that of the austenitic FeAlMnC or dual-phase FeAlMnCrC alloys. However, although the corrosion behaviors of the austenitic FeAlMnCrC alloys have been studied, all of their examinations were only focused on the alloys with Cr $\leq$ 3.0%. Information concerning the corrosion behaviors of the FeAlMnCrC alloys with higher Cr content is very deficient. Therefore, the purpose of this study is an attempt to examine the electrochemical corrosion properties of four austenitic Fe-9%Al-30%Mn-(3,5,6.5,8)%Cr-1%C alloys.

2. Experimental Procedure

The chemical compositions of the alloys are shown in Table 1. The alloys were prepared by melting commercial pure Fe, Al, Mn, Cr and carbon powder in an induction furnace under a controlled protective argon atmosphere. After being homogenized at 1473 K for 24 h, the ingots were sectioned into 5-mm thick slices. These slices were subsequently solution heat-treated in vacuum furnace at 1373 K for 2 h and then rapidly quenched into room-temperature water. Potentiodynamic polarization curves were measured in 3.5% NaCl solution at 298 K. Electrochemical polarization curves were obtained by using an EG&G Princeton Applied Research Model 273 galvanostat/potentiostat. Specimens with an exposed surface area of $\sim$1 cm^2 were ground with 2000-grit SiC paper and then with 1.5 μm Al_2O_3 powder,

Table 1 Chemical compositions of the present alloys (mass%).

Alloy	Fe	Al	Mn	Cr	C
A (3Cr)	Bal.	8.89	29.35	3.03	0.94
B (5Cr)	Bal.	8.93	29.76	4.92	1.07
C (6.5Cr)	Bal.	9.06	30.23	6.56	1.04
D (8Cr)	Bal.	8.97	29.27	8.06	1.05

*[1]Graduate Student, National Chiao Tung University. Present address: Department of Materials Science and Engineering, 1001 Ta Hsueh Road, Hsinchu 30049, Taiwan, R. O. China

*[2]Corresponding author, E-mail: tfliu@cc.nctu.edu.tw; chengshun.mse86g@nctu.edu.tw

washed in distilled water and rinsed in acetone prior to passivation. Potentiodynamic polarization curves were obtained at a potential scan rate of 5 mV/s from −1 V to 0.5 V. The concentration of elements in the passive film was examined by Auger electron spectroscopy (AES) and X-ray photoelectron spectroscopy (XPS). The AES spectrum measurements were performed with a LAS-3000 combined AES/XPS/SIMS surface analysis system using a Al Kα ray source ($h\nu = 1486.6$ eV). The background pressure in the sample chamber was about 2×10^{9} Torr (3×10^{-7} Pa). The energy of the primary electron beam and the Al^{+} sputtering beam are 3 and 1.5 keV, respectively. The Auger peaks recorded were Fe (703 eV), Al (1394 eV), Mn (542 eV), Cr (529 eV), O (503 eV) and C (272 eV). The sputtering rate was calibrated to be 0.25 nm/min by ion etching of a Ta sample covered with Ta_2O_5 film of known thickness. Microstructures were examined by using optical microscopy and transmission electron microscopy (TEM). TEM specimens were prepared by means of a double-jet electropolisher with an electrolyte of 15% perchloric acid, 25% acetic acid and 60% ethanol. Electron microscopy was performed on JEOL-2000FX TEM operating at 200 kV. The energy-dispersive X-ray spectrometry (EDS) was used to analyze the compositions of phases.

3. Results and Discussion

Optical microscopy examinations indicated that the as-quenched microstructure of the alloys A (3Cr) and B (5Cr) was single-phase austenite. An example is shown in Fig. 1(a). No precipitates could be detected in the alloys A (3Cr) and B (5Cr), which was confirmed by electron microscopy. This seems to imply that the Cr could be completely dissolved within the austenite matrix at 1373 K as Cr $\leq$ 5%. Figure 1(b), an optical micrograph of the alloy C (6.5Cr), reveals that some precipitates could be observed within the austenite matrix and on the grain boundaries. With increasing the Cr content, the amount of the precipitates increased, as shown in Fig. 1(c).

Figure 2 shows the potentiodynamic polarization curves for the four alloys in 3.5% NaCl solution. Table 2 is the summary of electrochemical parameters. In Fig. 2, it is clear that passivation could be observed for all alloys, and the broad passive region increased as Cr content increased from 3 to 5% and decreased as Cr content up to 6.5 and 8%. With different Cr content, the E_{corr} of the alloys was varied from −721 mV to −560 mV. Alloy B (5Cr) has the noblest E_{corr} (−560 mV). Moreover, with increasing the Cr content from 3 to 5%, the E_{pp} was pronouncedly increased from −220 mV to −53 mV. However, with further increasing the Cr content to 6.5 and 8%, E_{pp} became more negative. The results indicate that alloy B (5Cr) had the highest resistivity to pitting damage.

The depth-concentration profiles for the passive film formed on the four alloys in 3.5% NaCl solution were examined by AES/XPS. Figure 3 indicates the Auger depth profiles of the passive film formed on the alloys A (3Cr), B (5Cr) and C (6.5Cr). The detection of carbon element on the outmost layer may be due to surface contamination. Compared concentrations of elements in the passive film

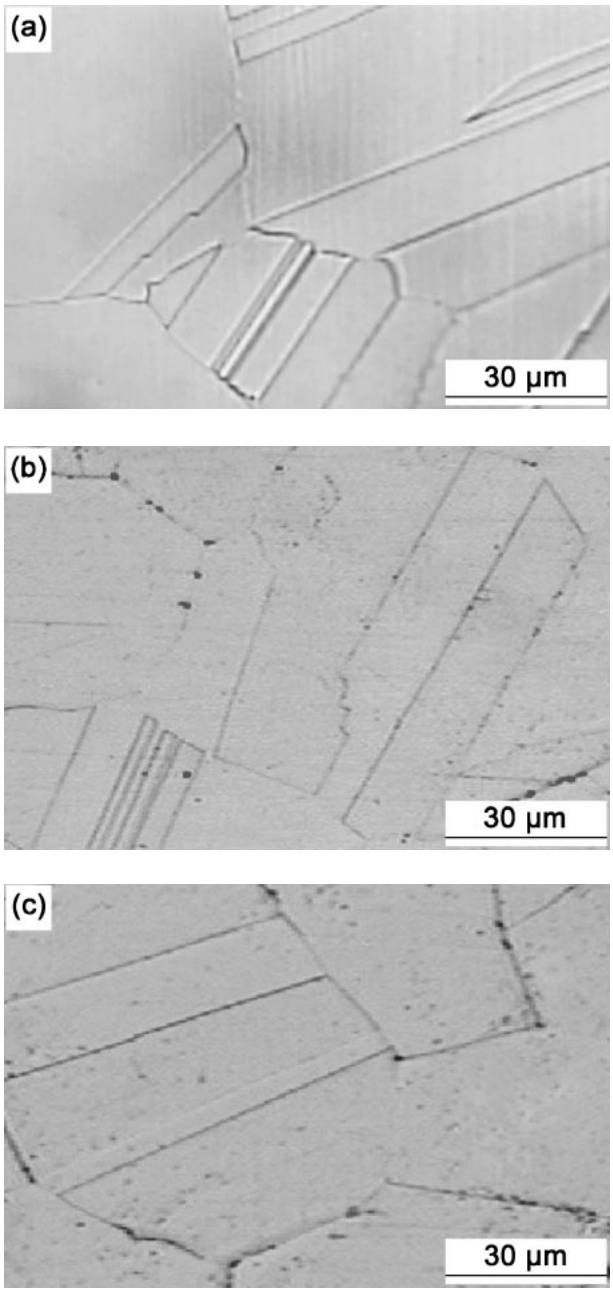

Fig. 1 Optical micrographs of the Fe-9%Al-30%Mn-(5,6.5,8)%Cr-1%C alloys. (a) 5 Cr, (b) 6.5 Cr, and (c) 8 Cr.

with those in matrix, it is obviously seen that the Mn and Fe contents abruptly decreased in the passive film. In contrast, Cr and Al contents were reverse tendency. This indicates that Cr and Al enrichment was attributed to the preferential dissolution of unstable oxides of Mn and Fe into electrolyte solution, and then replacement by Cr and Al within the oxide layer. There were broad peaks of Cr and Al at a depth of 0 to 2 nm, which corresponded with the peak of O. Compared to the previous studies of corrosion behaviors of FeAlMnC alloys, the increase of Cr and Al in oxides is likely to be responsible for the improved stability of the passive film.

Although the formation of Cr and Al oxides in the passive film can explain the beneficent effect on corrosion behaviors of adding Cr into FeAlMnC alloys,[6,12,13] the AES analysis can not explain the reason why the E_{corr} of alloys C (6.5Cr)

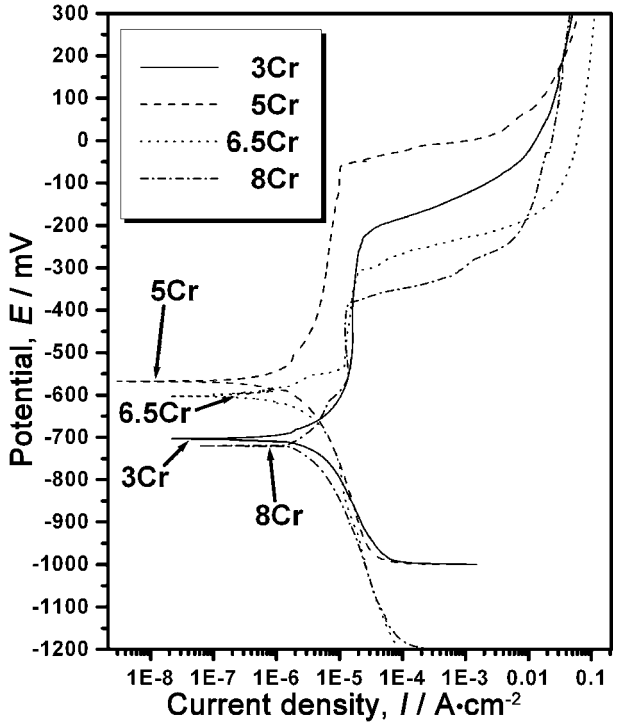

Fig. 2 Potentiodynamic polarization curves for the four Fe-9%Al-30%Mn-(3,5,6.5,8)%Cr-1%C alloys in 3.5% NaCl solution.

Table 2 The electrochemical parameters from potentiodynamic polarization curves for the four Fe-9%Al-30%Mn-(3,5,6.5,8)%Cr-1%C alloys in 3.5% NaCl solution.(*)

Alloy	Electronchemical Parameters from Polarization Curves			
	E_{corr} (mV)	E_{cr} (mV)	E_{pp} (mV)	I_p (A·cm^{-2})
A (3Cr)	−703	−550	−220	2.47E−05
B (5Cr)	−560	−520	−53	9.96E−06
C (6.5Cr)	−601	−534	−308	1.99E−05
D (8Cr)	−721	−564	−380	1.68E−05

(*)E_{corr}, corrosion potential; E_{cr}, critical potential for active-passive transition; E_{pp}, pitting potential; I_p, passive current density, minimum value.

and D (8Cr) decreased (more negative), as illustrated in Table 2. In order to clarify this feature, TEM examinations were undertaken. Figure 4(a) is a bright-field electron micrograph of alloy C (6.5Cr), clearly revealing the presence of the precipitate within the austenite matrix. Figure 4(b) is a selected-area diffraction pattern taken from the precipitate marked as "C" in Fig. 4(a). Compared to the previous literature,[18] it is obvious that the precipitate is $(Fe,Mn,Cr)_7C_3$ carbide with lattice parameters a = 1.3949 nm, and c = 0.4563 nm. Figures 4(c) and (d) represent two typical EDS profiles of the $(Fe,Mn,Cr)_7C_3$ carbide and the austenite matrix nearby the $(Fe,Mn,Cr)_7C_3$ carbide. The quantitative analyses of ten different EDS profiles indicated that the chemical composition of the carbide was Fe-1.9%Al-34.5%Mn-23.2%Cr (EDS with a thick-window detector is limited to detect the elements of atomic number of 11 or above; therefore, carbon cannot be examined by this method), and the chemical composition of the austenite

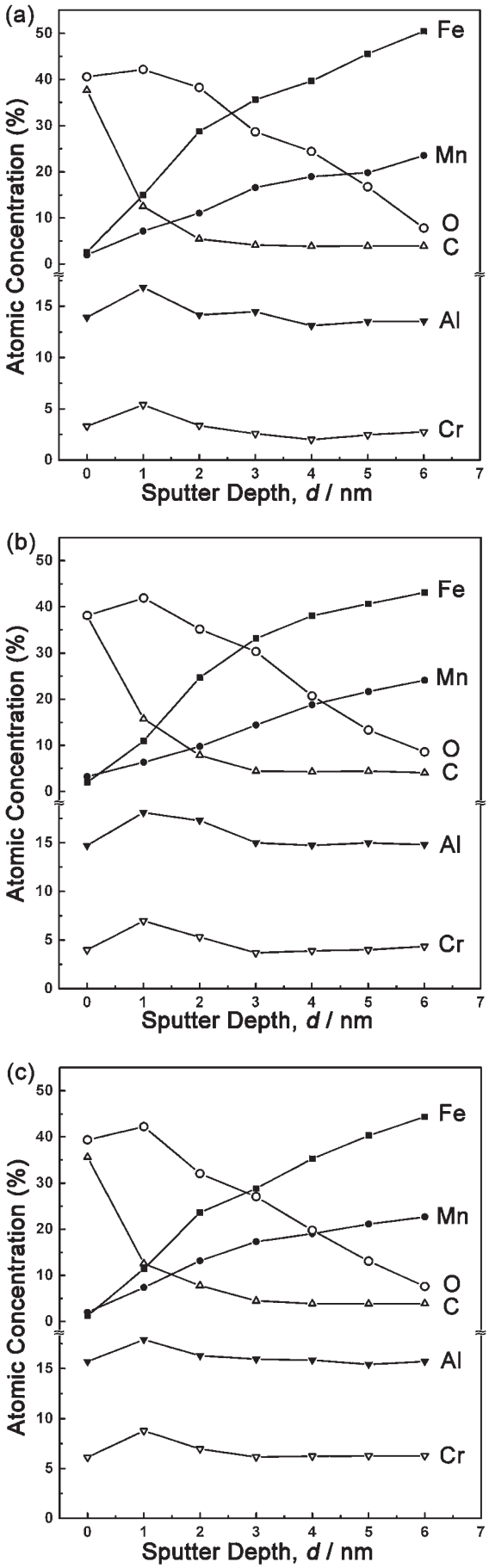

Fig. 3 AES depth profiles for the passive film of the Fe-9%Al-30%Mn-(3,5,6.5)%Cr-1%C alloys. (a) 3 Cr, (b) 5 Cr, and (c) 6.5 Cr.

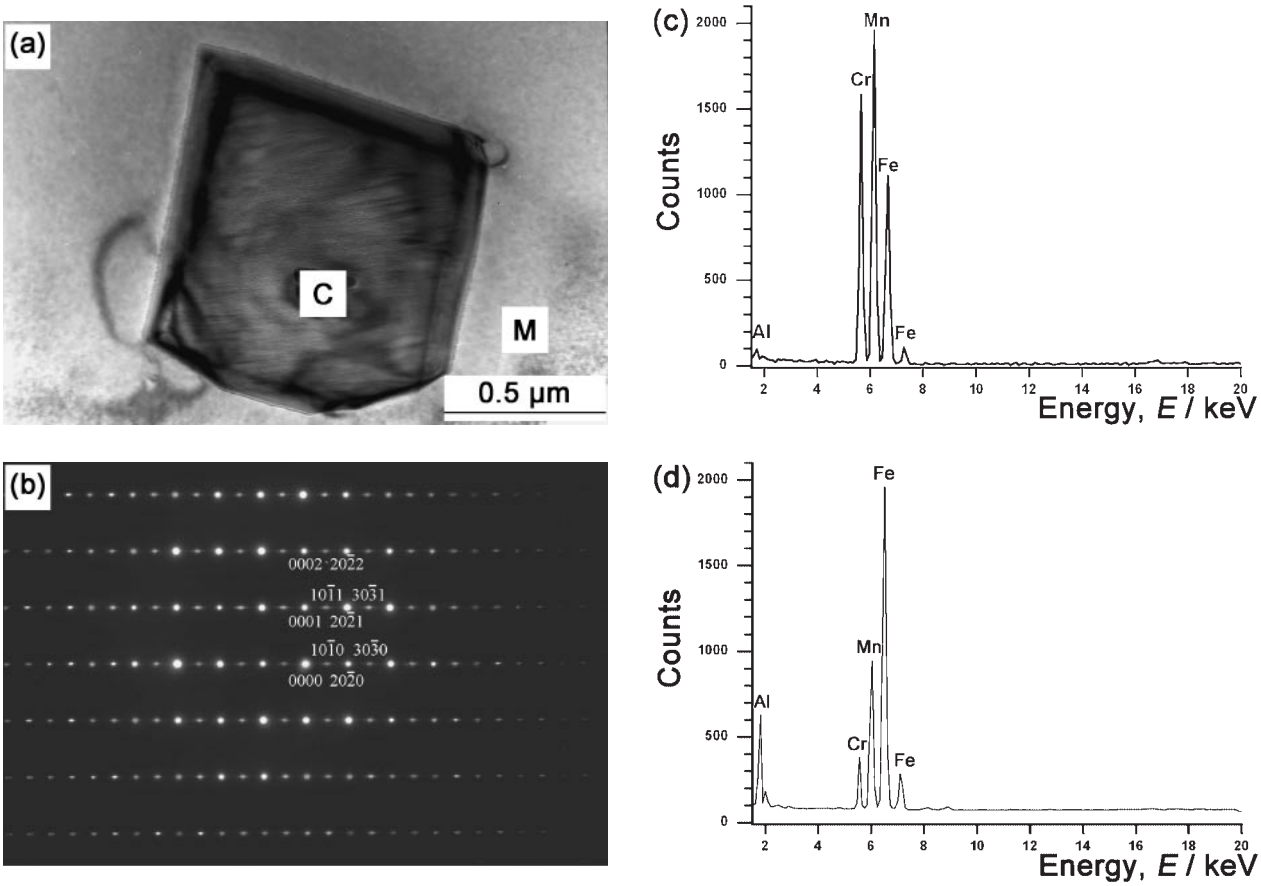

Fig. 4 Transmission electron micrographs of the as-quenched Fe-9%Al-30%Mn-6.5%Cr-1%C alloy. (a) bright-field, (b) a selected-area diffraction pattern taken from the $(Fe,Mn,Cr)_7C_3$ carbide marked as "C" in (a). The zone axis of the $(Fe,Mn,Cr)_7C_3$ carbide is $[2\bar{1}\bar{1}0]$. (c) and (d) two typical EDS profiles obtained from the $(Fe,Mn,Cr)_7C_3$ carbide marked as "C" and the austenite matrix nearby the $(Fe,Mn,Cr)_7C_3$ carbide marked as "M" in (a), respectively.

matrix nearby the carbide was Fe-9.7%Al-27.2%Mn-4.7%Cr. It is clearly seen that the concentration of Cr in the $(Fe,Mn,Cr)_7C_3$ carbide is up to 23.2%, which is much greater than that in the austenite matrix nearby the carbide. It is thus to anticipate that owing to the formation of Cr-rich $(Fe,Mn,Cr)_7C_3$ carbides, the Cr content within the austenite matrix should be pronouncedly decreased. As a consequence, the formation of Cr-rich $(Fe,Mn,Cr)_7C_3$ carbides resulted in the decreasing of E_{corr} and E_{pp} of the alloys C (6.5Cr) and D (8Cr).

By comparing with the previous studies, two important experimental results are worthwhile to note as follows. (I) In the previous studies concerning the corrosion behaviors of fully austenitic Fe-(8.3–9.3)%Al-(26.0–30.0)%Mn-(0.85–1.45)%C alloys in 3.5% NaCl solution,[9,10] it was reported that only narrow passive region could be observed, and the E_{corr} of the alloys was in the range from −920 to −790 mV. In the present study, it is clear that a broad passive region could be observed, for all of the present alloys, and the E_{corr} was from −721 to −560 mV. This demonstrates that the addition of Cr is indeed beneficial for the corrosion resistance of the austenitic FeMnAlC alloys in NaCl solution, which is in agreement with that reported by other workers in the austenitic FeMnAlCrC alloys.[5,6] (II) The present result indicates that the E_{corr} value for the alloy A (3Cr) was −703 mV, which is comparable to about −720 mV for the as-quenched Fe-8.4%Al-29.5%Mn-2.6%Cr-1.06%C alloy in 3.5% NaCl solution.[6] However, no information concerning the corrosion behaviors of the austenitic FeMnAlCrC alloys with Cr ≥ 3% in the NaCl solution has been provided in the previous literatures to compare.

4. Conclusions

The corrosion behaviors of the as-quenched Fe-9%Al-30%Mn-(3,5,6.5,8)%Cr-1% alloys in 3.5% NaCl solution have been examined.

(1) Both of the E_{corr} and E_{pp} increased as Cr content increased from 3 to 5%, and decreased as Cr content up to 6.5 and 8% due to the formation of Cr-rich $(Fe,Mn,Cr)_7C_3$ carbides in the austenite matrix and on the grain boundaries. This indicates that the alloy B (5Cr) exhibited the best corrosion resistance in 3.5% NaCl solution.

(2) Compared to the previous studies of the as-quenched austenitic FeAlMnCrC alloys with Cr ≤ 3%, the present result shows that the E_{corr} and E_{pp} would be pronouncedly increased as the Cr content was added up to 5%. The reason is that the 5% Cr could be completely dissolved within the austenite matrix at 1373 K.

Acknowledgments

The authors are pleased to acknowledge the financial support of this research by the National Science Council, Republic of China under Grant NSC95-2221-E-009-086-MY3.

REFERENCES

1) S. M. Zhu and S. C. Tjong: Metalls. Trans. A **29** (1998) 299–306.
2) W. K. Choo, J. H. Kim and J. C. Yooh: Acta Mater. **45** (1997) 4877–4885.
3) I. S. Kalashnikov, O. Acselrad, T. Kalichak, M. S. Khadyyer and L. C. Pereira: J. Mater. Eng. Perf. **9** (2000) 334–337.
4) S. C. Chang and Y. H. Hsiau: J. Mater. Sci. **24** (1989) 1117–1120.
5) S. C. Chang, J. Y. Liu and H. K. Juang: Corrosion. Eng. **51** (1995) 399–406.
6) S. C. Chang, W. H. Weng, H. C. Chen, S. J. Lin and P. C. K. Chung: Wear **181–183** (1995) 511–515.
7) S. C. Tjong and C. S. Wu: Mater. Sci. Eng. **80** (1986) 203–211.
8) S. C. Tjong: Surface and Coatings Technology **28** (1986) 181–186.
9) W. T. Tsai and J. B. Duh: J. Mater. Sci. **22** (1987) 3517–3521.
10) J. B. Duh, W. T. Tsai and J. T. Lee: Corrosion **Nov** (1988) 810–818.
11) X. M. Zhu and Y. S. Zhang: Corrosion **54** (1998) 3–12.
12) C. J. Wang and Y. C. Chang: Mater. Chem. Phy. **76** (2002) 151–161.
13) M. Ruscak and T. P. Perng: Corrosion **Oct** (1995) 738–743.
14) S. T. Shih and C. Y. Tai: Corrosion **Feb** (1993) 130–134.
15) I. F. Tsu and T. P. Perng: Metall. Trans. A **22** (1991) 215–224.
16) C. C. Wu, J. S. Chou and T. F. Liu: Metall. Trans. A **22** (1991) 2265–2276.
17) S. M. Zhu and S. C. Tjong: Scripta **36** (1997) 317–321.
18) F. Ernst, Y. Cao and G. M. Michal: Acta Mater. **52** (2004) 1469–1477.